Improved Limb Atmospheric Spectrometer II (ILAS-II) Version 1.4 retrieval algorithm for the gas and aerosol profiles in the stratosphere

T. Yokota[1], H. Nakajima[1], T. Sugita[1], H. Kawasaki[2], M. Horikawa[2], H. Matsuda[2], N. Uemura[2], H. Kanzawa[1*], H. Kobayashi[1**], and Y. Sasano[1]

[1]National Institute for Environmental Studies, Tsukuba, Ibaraki, Japan

[2]Fujitsu F.I.P. Corporation, Tokyo, Japan

Short title: ILAS-II Version 1.4 retrieval algorithm

[*] Now at Graduate School of Environmental Studies, Nagoya University, Nagoya, Japan

[**] Now at Central Research Institute of Electric Power Industry, Tokyo, Japan

Abstract.

Improved Limb Atmospheric Spectrometer II (ILAS-II), a sensor for stratospheric ozone layer observation using a solar occultation technique, was mounted on Advanced Earth Observing Satellite II (ADEOS-II), which was put into a sun-synchronous polar orbit in December 2002. ILAS-II measured 5,890 vertical profiles of several gas concentrations over high latitude regions from January to October 2003. This paper describes the ILAS-II data processing algorithm of Version 1.4 used to retrieve vertical profiles of gases such as ozone, nitric acid, nitrous oxide, and methane from the infrared spectral measurements and those of aerosol extinction coefficients at 780 nm from the visible spectral measurements. To derive simultaneously mixing ratios of individual gas species as a function of altitude, a nonlinear least squares method was utilized for the spectral fitting, and an onion peeling method was applied to the vertical profiling. In this way, the ILAS-II Version 1.4 algorithm is similar to the ILAS Version 5.20 algorithm. This paper emphasizes the differences between the two retrieval algorithms.

This paper also discusses an estimation of errors, repeatability errors and external errors, associated with the derived gas profiles in detail. This paper, moreover, carried out numerical simulations to investigate performance of the non-gaseous contribution correction technique, showing that the background level of sulfuric acid aerosols has little effect on the

retrieved profiles, while some kinds of polar stratospheric clouds (PSCs) with extinction coefficients of the order of 10^{-3} km^{-1} at a wavelength of 780 nm have non-negligible effects on the profiles of some gas species, as shown in the ILAS Version 5.20 case.

1. Introduction

Improved Limb Atmospheric Spectrometer II (ILAS-II), aboard Advanced Earth Observing Satellite II (ADEOS-II which was given a new name Midori-II after the successful satellite launch on December 14, 2002), measured the stratospheric ozone layer in the high latitude regions of both northern and southern hemispheres (54-71^{o}N and 64-88^{o}S) on the basis of the solar occultation technique from January to October, 2003. ADEOS-II is a polar-orbiting satellite which carried Global Imager (GLI), Advanced Microwave Scanning Radiometer (AMSR), Polarization and Directionality of the Earth's Reflectances (POLDER), and Sea Winds besides ILAS-II. The descending equator-crossing time of the satellite was 10:30 am, its inclination angle and satellite altitude were 98.7 degrees and about 810 km, respectively [*JAXA EORC Ed.*, 2005].

The ILAS-II instrument is a successor of ILAS [*Sasano*, 2002], both of which were developed by the Ministry of the Environment of the Japanese Government for the purposes of stratospheric ozone layer observations. Main targets of the ILAS measurements were vertical concentration profiles of O_3, HNO_3, NO_2, N_2O, CH_4, and H_2O, and that of aerosol extinction coefficient (AEC, hereafter) at 780nm. ILAS had two spectrometers: infrared (IR, 6.21-11.76 μm) and visible (VIS, 753-784 nm) spectrometers. On the other hand, ILAS-II had four spectrometers by adding a mid-infrared (MIR, 3.00-5.70 μm) spectrometer for

precise measurements of the ILAS target species and a high resolution infrared spectrometer (12.78-12.85 μm) for $ClONO_2$ measurements [*Nakajima et al.*, 2005].

ILAS-II had a new function in the IR and MIR spectrometers to select either a direct current (DC) or an alternating current (AC) data acquisition mode, the former of which is for DC outputs after and the latter for AC outputs before passing through a lock-in amplifier [*Nakajima et al.*, 2005]. The use of the AC mode data is expected to give higher vertical resolution than the data obtained by the DC mode, because the DC mode signals pass through lock-in amplifiers and are averaged in time responses.

In addition, some modifications were made to the ILAS-II instrument, which includes slits for light entrance narrower than that of ILAS for better vertical resolution, projection of slit locations on the solar disk detected by the one-dimensional sun-edge sensor (SES) for more precise determination of tangent heights, improvement of effective spectral resolution in the VIS spectrometer for more precise pressure and temperature retrieval, and exoatmospheric measurements of brightness distribution on the solar disk with an additional sun-scanning function for identifying sun-spots and solar limb darkening effects.

The slit image projection on the sun image, obtained by the SES, was realized by putting a reflective optics with two light entrance slits at the focusing position of the telescope [*Nakajima et al.*, 2005]. However, unexpected distortions were found in output signals

from the IR and MIR spectrometers and the SES, the cause of which was likely to be thermal deformation in the slit portions in the real measurement situations on orbit. Because of this, some data processing functions such as the limb darkening effect correction, the sun spot effect correction, and the precise tangent height determination were not utilized in such a way as planned.

This paper describes data processing algorithm Version 1.4 which has been used for generating ILAS-II products of O_3, HNO_3, N_2O, CH_4, and AEC at 780 nm for distribution to the public as well as their error information. Other gas products are not opened to the public because some of them expose unexpected features and they need further investigation as well as validation.

The ILAS-II Version 1.4 algorithm, which basically inherited the ILAS Version 5.20 algorithm [*Yokota et al.*, 2002], was developed for processing data from the IR and the VIS spectrometers of ILAS-II. However, some improvements were made such as an addition of pre-processing of the AC mode data, updates of spectrometric database and climatological database, and so on. The “repeatability error” is introduced to the “total error” estimation instead of the “internal error” which was used in the ILAS Version 5.20 algorithm.

It is expected that retrieved gas profiles may contain artificial systematic errors under the conditions of high density aerosols including Polar Stratospheric Clouds (PSCs) as it was

found in the ILAS Version 5.20 products. This is caused by the use of the non-gaseous contribution correction technique adopted both in the ILAS Version 5.20 and the ILAS-II Version 1.4 data processing. The technique is based on a linear interpolation of aerosol extinction coefficients inferred at four window elements of the IR spectrometer when estimating contribution of the spectrum due to aerosols and PSCs [*Yokota et al.*, 2002]. By using numerical simulations, this paper demonstrates magnitudes of the expected systematic errors which are caused by the non-gaseous contribution correction.

In Section 2, an overview of the ILAS-II instrument and measurement flow is provided. In Section 3, data processing details such as the signal pre-processing, the tangent height determination, and the calculation of atmospheric transmittance are described. Major characteristics of the retrieval methods, compared with the methods of the ILAS Version 5.20, are summarized in Section 4. Section 5 describes the error estimation method and results of error estimation using synthesized ILAS-II data as well as results of the systematic errors due to the non-gaseous contribution correction. A summary is given in Section 6.

2. An Overview of the ILAS-II instrument and Measurement Flow

An overview of the ILAS-II instrument and data characteristics is very briefly given here because their details are provided elsewhere [*Nakajima et al.*, 2005].

ILAS-II measurements are based on a solar occultation technique with four spectrometers to measure atmospheric transmittance and a device to detect positions of lower and upper edges of the sun as the principal optical components (see Table 1). The IR spectrometer covers a wavelength region from 6.21 to 11.76 μm with a 44-element $PbTiO_3$ pyroelectric detector array while the MIR spectrometer covers from 3.00 to 5.70 μm with a 22-element detector array. The high resolution infrared spectrometer covers wavelengths only from 12.78 to 12.85 μm, which is dedicated to $ClONO_2$ measurements. The VIS spectrometer uses a metal-oxide semiconductor (MOS) diode detector array with 1024 elements and covers 753 - 784 nm in wavelength.

Table 1

The ILAS-II instrument is equipped with devices for tracking the sun and with the SES for precisely determining positions of the instantaneous field of view (IFOV). The latter is a one-dimensional MOS photodiode array to detect the upper and lower edges of the sun along the vertical direction of a diameter which is intercepted by a plane containing the brightness center of the sun, the satellite, and the center of the earth. The SES also detects the position of the IFOV of each spectrometer, which is used for determining tangent heights together with geometric information on the satellite, the earth, and the sun [*Tanaka et al.*, 2005].

ILAS-II measurement flow charts for the occultation events corresponding to a sunrise

and a sunset seen from the satellite together with the IR and VIS data are shown in Figure 1. Fig. 1

For a sunrise event which occurs in the northern hemisphere, measurements are performed by the following sequence: pointing to a fixed location inside of the instrument, the deep space (a), and tracking the brightness center of the sun through the atmosphere (b) and in the exoatmosphere (c), followed by scanning of the sun (d), and then again pointing to the deep space and to a fixed location in the instrument (e). For a sunset event in the southern hemisphere, the measurement sequence is in the reverse mode, and tracking the brightness center of the sun in the exoatmosphere (c) is done before scanning of the sun (d) followed by tracking the brightness center of the sun through the atmosphere (b) (see Figure 1).

3. Data Processing

The fundamental flow of the data processing in the ILAS-II Version 1.4 algorithm is similar to that of the ILAS Version 5.20 [*Yokota et al.,* 2002], where the pre-processing of raw data, the tangent height determination, the retrieval of temperature, pressure and AEC profiles from the VIS spectrometer data, and the retrieval of gas profiles are carried out in this order. As mentioned later, however, the temperature and pressure products derived from the ILAS-II data are not used but the stratospheric assimilation data from the United Kingdom Meteorological Office (UKMO) [*Swinbank and O'Neil*, 1994; *Lorenc et al.,* 2000]

and climatological data from COSPAR International Reference Atmosphere (CIRA) [*Rees et al*., 1990] are introduced as temperature and pressure information for gas profile retrievals. Therefore, retrievals of temperature and pressure and of AEC at 780 nm are independent from gas retrievals, thus making their parallel processing possible, which is also the same as in the ILAS Version 5.20 data processing.

Data levels are defined as follows: Level 0 (L0) for the whole raw data, L0a for the data extracted from the whole data stream for further data processing, L1 for the pseudo-transmittance data, L1a for the data after solar limb darkening and sun-spot effect corrections, and L2 for retrieved data products.

The original design of the IR data processing with regard to temperature and pressure information for gas retrievals had been to use temperature and pressure information derived from ILAS-II VIS spectrometer data. Because the retrieval of temperature and pressure, however, has not been successfully conducted yet [*Sugita et al.*, 2004], the UKMO assimilation data of temperature and pressure which is interpolated to locations and times of ILAS-II measurements are used for ILAS-II Version 1.4 data processing. The pressure and temperature, in the regions of upper atmosphere where the UKMO assimilation data do not cover, are given by the CIRA 1986 model data.

A climatological data set for gas profiles for every month and every latitude band (10

degrees width) is used as initial values for the gas retrievals, and is used for gas absorption calculations for non-gaseous contribution correction and for external error estimation, which will be described later. The climatological data was statistically generated from observations by other satellite-borne instruments, as is detailed by Appendix A of *Yokota et al.* [2002]. The updates from *Yokota et al.* [2002] include COF_2 and CO_2 data calculated from the Atmospheric Trace Molecule Spectroscopy (ATMOS) Version 3 data set [*Irion et al.*, 2002], and the CO_2 climatological data modified by adding 1.5 ppmv uniformly to the ATMOS Version 3 data.

The cross-talk between the adjacent detector array elements for the ILAS-II instrument has been modeled and incorporated into an instrument function for each element in advance; while that for ILAS was expressed by a simple equation and applied in the ILAS data processing sequence. As the detector of element number 44 (at 11.76 μm) of the ILAS-II IR spectrometer was found to be affected by stray lights with wavelength shorter than that of the element number 1 (at 6.21 μm), the radiance calculation within the detector of element number 44 took this effect into consideration theoretically.

A total of 6,029 occultation events (OEs) was scheduled to make measurements during a test operation period from January to March 2003 and during a continuous operation period from April to October 2003; and actual measurements were conducted for a total of 5,890

OEs. Among them, a total of 5,833 OEs data was properly processed, and a total of 5,614 OEs products was selected in terms of data quality and has been provided to researchers registered to the ILAS-II project.

3.1 Signal pre-processing

A basic pre-processing includes data extraction, outlier treatment, trend correction, solar limb darkening correction, and sun-spot effect correction in the processing sequence from L0 to L0a, L1, and L1a. The L0 data consists of sequences of output signals called “frame data”, which was gathered with a 10 Hz sampling rate from the spectrometers. Since generation of L0a data (extraction of effective data sequence for further data processing) requires tangent height information for each frame data, tentative tangent height calculation is made using a model atmosphere for ray path calculation. A median filter is used for detecting and correcting spike noise in the L0a data. The trend in the signals in one occultation measurement is corrected by interpolation and extrapolation with linear trend equations that have been determined from the data of the deep space (0%) and the direct sun (100%) signals.

A pre-processing specific to the ILAS-II IR spectrometer data is an AC mode processing. When the output signal is obtained by a DC mode, the signal experiences

temporally-weighted convolution, thus requiring deconvolution as pre-processing in the same way as in ILAS Version 5.20. On the other hand, the AC mode output signal as shown in Figure 2 needs to be converted to instantaneous signal equivalent to the DC mode signal. The following Equation (1) is applied to four data points sampled with 90 degree intervals in a phase of the AC signal, because the original output signal is modulated by a chopper blade into an AC signal:

Fig. 2

$$A = \frac{\sqrt{(I_a - I_c)^2 + (I_b - I_d)^2}}{2}, \quad (1)$$

where A is an effective amplitude, and I_a, I_b, I_c, *and* I_d are intensities sampled at four phases in one cycle of the AC signal.

Since the AC outputs do not pass through the lock-in amplifier, as the DC outputs do, but pass only through the pre-amplifier, a time constant of the AC signal response is one fifth as small as that of the DC signal. This advantage enables the signal response to be well approximated not by the weighted convolution but by a simple time delay, leading to a simple estimation of instantaneous signal only by a time delay correction.

L1 data as pseudo-transmittance τ_t is generated by applying the following Equation (2) to the signal x_t obtained when the spectrometer was looking through the atmosphere:

$$\tau_t = \frac{x_t - x_0}{x_{100} - x_0}, \tag{2}$$

where x_0 is the estimated signal at time *t* by interpolating the data looking at the deep space before and after the atmospheric measurements, and x_{100} is the estimated signal at time *t* by extrapolating the data looking at the sun before or after the atmospheric measurements. These data interpolation and extrapolation are adopted for precise transmittance calculation by considering temporal trends of the signals x_0 and x_{100} during one OE. . As for the VIS spectrometer data, L1a data is the corrected L1 data of solar limb darkening and sun-spot effects. On the other hand, L1a is just the same data as L1 for the IR and the MIR spectrometers, because solar limb darkening and sun-spot effect corrections are not applied to them as described in Section 3.3.

A low pass filter with a cut-off frequency of 0.5 Hz is applied to 21 consecutive frame data of L1a for smoothing in the same way as in ILAS. For the L1a data around the lowest height level of atmospheric measurements, the number of frames for the low-pass filter to be applied is made variable to adjust weights of the filter to keep the cut-off frequency as 0.5 Hz, so that the measurement data would be utilized at as low height levels as possible.

The IFOVs correspond to a spatial extent of 1.0 km (vertical) and 13.0 km (horizontal) at

tangent points for the IR and MIR spectrometers and to that of 1.0 km and 2.0 km for the VIS spectrometer. Effective vertical resolutions of measurements can be defined basically by those sizes of IFOV with the smoothing mentioned above. Moreover, the signal was continuously sampled at 10 Hz, but the spatial sampling interval was modulated by atmospheric refraction. Therefore, the more minute signals (about 120-200 m in the vertical interval) were measured in the lower atmosphere (about at 15-25 km) than those signals (about 300 m in the vertical interval) in the upper atmosphere (about at 40 km and above). This affects the data smoothing and vertical resolution of the data. Totally, the effective vertical resolutions are about 1.3 km at a tangent height of 15 km, 1.6 km at 20 km, 1.9 km at 25 km, 2.1 km at 30 km, 2.5 km at 40 km, and 2.8 km at 50 km (see Figure 3).

Fig. 3

3.2 Tangent height determination

Basically, the same procedure as that of ILAS [*Nakajima et al.*, 2002] is applied to tangent height determination in the ILAS-II Version 1.4 algorithm, where used is the information on geometric relationship between the earth and the sun at a ILAS-II measurement time, the satellite position relative to the earth, and direction of the spectrometer's IFOV as well as the meteorological data for temperature and pressure profiles.

A major difference from the ILAS algorithm is that the information on the entrance slit position on the sun image is used to calculate positions of the IFOVs on the solar disk. Difficulties, however, have arisen regarding the determination of tangent heights for all the data sequence in real situations, because signals from the SES seemed different from our expectations based on the original instrument designs. As an alternative, the method to use information on the lower edge position of the sun is applied to the tangent height regions at and above 30 km while the method to compare oxygen *A*-band transmittance spectra theoretically calculated with those observed is applied to the region below 30 km. Details of the tangent height determination methods are described by *Tanaka et al.* [2005], who concluded that the uncertainties of the tangent height determined are about +/-180 m of bias error and about +/-30 m of random error.

3.3 Theoretical calculation of transmittance

<Layering>

Unknown parameters of gas concentration and AEC at 780 nm are retrieved at tangent heights which are defined as boundaries of atmospheric layers with 1 km thick. Distributions of gas concentrations and AEC in the 1 km-thick layer are assumed to have linearly distributed when calculating transmittance along light ray paths. L1a data of the

ILAS-II at a layer boundary, after the data smoothing, is given by interpolation from two frame data corresponding to just above and below the boundary height concerned.

Two major differences from the ILAS Version 5.20 algorithm are to put the unknown parameters on the layer boundaries and to start profile retrievals from an additional 1 km-thick dummy layer outside the targeted height region. Since this dummy layer is supposed to absorb contribution from all the atmospheric layers above, the results look too unreasonable to use scientifically in general, and therefore they are not included in the products.

To derive gas concentration profiles, a spectral fitting method is applied to minimize residuals between transmittance spectra observed and those calculated theoretically. The onion-peeling method is applied for vertical inversions. Theoretical calculations are also made at the layer boundaries defined.

<Transmittance calculation>

Optical thickness in the infrared region is calculated in the same as before on the basis of the radiative transfer theory [*Yokota et al.*, 2002]. The major changes from the ILAS Version 5.20 algorithm are: the high-resolution transmission molecular absorption database (HITRAN): edition of 2000 [*Rothman et al.*, 2003] is used instead of HITRAN 1996

[*Rothman et al.*, 1998] for line parameters, the CKD 2.4 of LBLRTM 5.21 is used instead of CKD 2.1 [*Clough et al.*, 1989], and the calculation of transmittance is carried out with an interval of 0.001 cm^{-1} instead of 0.002 cm^{-1}. Calculations of optical thickness related to the VIS spectrometer measurements are described in Section 4.

As for the high-resolution solar source function data, which includes Fraunhofer lines of the solar atmosphere and is used for theoretical spectral data, Kurucz [1992] data from a data file of LBLRTM was used for the IR spectrometer. On the other hand, a high-resolution solar spectrum, newly obtained from a balloon measurement [*Camy-Peyret et al.*, 2001], was used for the VIS spectrometer.

Up to the ILAS Version 5.20, the cross section table of $ClONO_2$ in the HITRAN database was used in calculating absorption coefficients. However, the calculation was changed to use a look-up table (P-T Table) of cross sections, which was calculated at typical combination grids of pressure and temperature by using the pseudo-line parameters offered by G. C. Toon (unpublished data, 1995, 2000) based on the data of *Wagner and Birk* [2003].

<Solar limb darkening and sun-spot effect corrections>

When looking at the sun through the atmosphere from the satellite, the sun image is squashed vertically because of atmospheric path refraction. This makes the apparent size of

the IFOV relative to the sun increase as the tangent height of measurement decreases, resulting in different contribution of the solar limb darkening and sun-spot effects to the spectrometer signals depending on the tangent height.

In the ILAS Version 5.20 algorithm [*Yokota et al.*, 2002], the solar limb darkening effect was taken into consideration on the basis of estimation with an empirical equation from literatures. On the other hand, ILAS-II obtained information on the brightness distribution on the solar disk by making a sun scan in the exoatmosphere (i.e., (d) in Figure 1) with the spatial resolution of the IFOVs during every measurement sequence. The information obtained by this way is used for correction of the limb darkening effect in the VIS spectrometer data processing.

The sun scan signals from the IR spectrometer are distorted so much (see (d) in the top charts of Figure 1) owing to the thermal distortion of the entrance slit that they are not used for the correction of the IR spectrometer data. Even an empirical equation is not utilized for the IR signal corrections. Estimated bias errors in the retrieved gas profiles caused by neglecting the solar limb darkening effects are less than about 0.5 % for HNO_3, less than about 1 % for O_3 and N_2O, and less than about 3 % for CH_4 for the altitude regions below 30 km where the limb darkening effect appears relatively strongly. Correction of the sun-spot effect on the IR data is not also taken into consideration in the ILAS-II Version 1.4 data

products for the same reason of the distortion of the IR sun scan data. Evidently, the sun-spots resulted in the abnormal profile features of N_2O, CH_4, and other species during 22-24 October, 2003 [see *Ejiri et al.,* 2005].

4. Retrieval Methods

<AEC distribution>

The algorithm for retrieving AEC profiles at 780 nm from the VIS spectrometer data is basically the same as that in the ILAS Version 5.20 data processing [*Hayashida et al.*, 2000; *Yokota et al.*, 2002]. Transmittance spectra obtained with the VIS spectrometer are contributed by absorption due to ozone Wulf band and oxygen *A*-band in addition to extinctions due to the Rayleigh scattering by air molecules and the Mie scattering by aerosols including PSCs. Taking advantage of its absorption spectra shape, contribution by ozone can be estimated by baseline fitting to the wavelength region where no absorption due to the oxygen molecules is expected.

For the wavelength region around 780 nm where no absorption of oxygen exists, subtracting the contribution of ozone absorption from the total transmittance gives the contribution of the Mie scattering by aerosols and that of the Rayleigh scattering by air molecules. Signals averaged over twelve elements around 780 nm is utilized for this

calculation. A set of optical thickness data derived from the transmittance at 780 nm along each ray path with a vertical distance of 1 km is solved to give vertical profiles of optical thickness per unit length, i.e. total extinction coefficient due to aerosols and air molecules, by applying the Levenberg-Marquart nonlinear least square method with the use of a matrix of ray path lengths. The AEC is finally derived by subtracting the Rayleigh scattering contribution estimated theoretically with the use of the UKMO temperature and pressure data from the total extinction.

<Gas concentrations>

Retrieval targets by the ILAS-II Version 1.4 algorithm are the AEC at 780 nm, the AECs at the four window elements of the IR spectrometer (7.12, 8.27, 10.60, and 11.76 μm in wavelength), and O_3, HNO_3, NO_2, N_2O, CH_4, H_2O, CFC-11, CFC-12, N_2O_5, and $ClONO_2$ as gas components. Among them, only the products of O_3, HNO_3, N_2O, CH_4, and AEC at 780 nm, which have been validated through comparison with other independent data sets [*Sugita et al.*, 2005; *Irie et al.*, 2005; *Ejiri et al.*, 2005; *Saitoh et al.*, 2005], are open to the public as well as their error information. Distribution of the other data products is suspended because some of them expose unexpected features and they have not yet been validated.

The algorithm to retrieve gas concentration profiles from the IR spectrometer data is

basically based on the spectral fitting and onion peeling inversion techniques, which is again the same as that of ILAS Version 5.20. More specifically, spectral fitting by the modified Levenberg-Marquart method is applied to the transmittance spectra sequentially from the top layer of the targeted atmosphere down to the bottom to solve volume mixing ratios (VMRs) of multiple gas species simultaneously.

Contributions to the light attenuation from other components than the gases, that is, aerosols and PSCs, are eliminated by the non-gaseous contribution correction method [*Yokota et al.*, 2002]. This method assumes that attenuation in the window elements, where absorption by gases is expected to be relatively small, is only due to aerosols including PSCs. Since small contribution due to gases, however, still remains, corrections are made utilizing the climatological data set for gas distributions. Transmittances at the wavelengths corresponding to the window elements thus determined provide vertical profiles of AECs by applying the same inversion technique as that of the AEC at 780 nm from the VIS spectrometer data. The AECs at other wavelengths are inferred by the linear interpolation and extrapolation of the window elements data.

The non-gaseous contribution correction is applied to the data in the height region below 40 km. It has been recognized that this correction method produces artificial systematic errors in gas profiles that cannot be neglected when there exists aerosols including PSCs of

high density [*Yokota et al.*, 2002], which will be further discussed in Section 5.2.

<Unexpected signals in IR spectrometer output>

Unexpected signal variation was observed in the output signals from IR and MIR spectrometers during the process of detailed analyses of products from the measurements by using the initial versions of data processing software. This variation in one occultation measurement was quit different from the signal simulation results before the ADEOS-II launch. Intensive analysis of the signal behavior and additional experiments using the ILAS-II Engineering Model of the instruments in a laboratory suggested that this phenomenon occurred possibly because of distortion of the entrance slit shape due to the thermal stress during sun-tracking phases. Accordingly, the output signals from the spectrometers are likely to have been distorted for measurements in high altitude regions when the sun light on the spectrometers was intense enough.

Degree of the distortion in the signals seems dependent on the observation modes (sunrise or sunset) and on tangent heights. The effects of the distortion are evidently seen only in the upper atmosphere above 25 km of the northern hemisphere (i.e, sunrise mode), and depend on the gas species. How it affects each product of gas profile retrievals is found in validation papers for each gas species *Sugita et al.* [2005] for O_3, *Irie et al.* [2005]

for HNO_3, and *Ejiri et al.* [2005] for N_2O and CH_4. The problem of thermal distortion of the entrance slit was also found in the SES outputs (see Section 3.2). Correction methods for the signal distortion are being studied.

5. Error Analysis

5.1 Repeatability error and external error

ILAS-II Version 1.4 data products (gas VMR profiles and AEC profiles) include error information represented by repeatability error and total error, for each altitude. The total error is defined as a root-sum-square of the repeatability error and the external error. Definitions of the external error and the repeatability error are described in the following.

External errors in the AEC at 780 nm are given by uncertainties in the Rayleigh scattering contribution because of uncertainties in temperature data. They are calculated through the variability of the Rayleigh scattering term with respect to the uncertainty of temperature: +/-2 degree given at 10 km, and +/-5 degree given at 70 km, with linear interpolation for intermediate altitudes for each measurement (Occultation Event, OE). Regarding external errors in gas products from the IR spectrometer data, representative error values were calculated in advance of the gas profile retrieval for every gas product and for every tangent height by giving temperature uncertainties of +/-2 degree at 10 km and +/-5

degree at 70 km, respectively, and by giving variability of climatological data for gas profiles which is used for the non-gaseous contribution correction. Details are found in *Yokota et al.* [2002].

According to *BIPM et al*. [1993], the term "repeatability of measurement results" is defined as the "closeness of the agreement between the results of successive measurements of the same object, carried out under the same condition." Hence, a repeatability index of ILAS-II measurements, approximated empirically using the following procedure, is introduced as a measure of precision. Note that the smaller value of the repeatability index represents the higher repeatability of the measurements. The repeatability index is estimated for every gas and for every tangent height from the minimum value in the ratios of the standard deviation to the mean value of the retrieved gas concentrations, which are calculated with data in the consecutive 100 OEs for every 50 OEs from April to October 2003 for each hemisphere. The repeatability index includes, therefore, uncertainties of the instrumental-origin and degrees of natural variability of the atmosphere. Assuming uncertainties of the instrumental-origin are constant in time, the minimum value of the ratios corresponds to a period of the lowest natural variability. Hence, the repeatability index is considered as an approximation of uncertainties of the instrumental-origin, i.e., as a measure of precision. The periods, when the smallest ratios manifest themselves, are dependent on

the gas species. Figure 4 demonstrates an example of the repeatability index, given as a relative value in percent, for O_3 in the northern hemisphere. Repeatability error for a certain VMR is calculated from the repeatability index for each gas multiplied by each retrieved VMR value. We put the minimum standard deviation of the VMRs in the repeatability index calculation procedure as a minimum threshold value of the repeatability error for each gas and for each altitude. For consistency, the repeatability error is also applied to obtain the errors in the AEC at 780 nm.

Fig. 4

Figures 5 and 6 show profiles of the repeatability error and the total error for each ILAS-II Version 1.4 product for the northern hemisphere and the southern hemisphere, respectively. As can be seen in these figures, the dominant contribution to the total error is from the repeatability error.

Fig. 5
Fig. 6

It should be noted that the internal error, which is calculated on the basis of residuals of the spectral fitting, was used instead of the repeatability error to estimate the total error in the ILAS Version 5.20 products. It was found, however, that since the internal errors included systematic errors especially in the sunrise data possibly owing to the inadequate spectroscopic parameters, the non-gaseous contribution correction, and effects of the entrance slit distortion, the internal errors are not legitimately regarded as random errors. Therefore, in the error estimation procedure of the ILAS-II Version 1.4, the repeatability

error is used as a measure of precision.

5.2 Systematic errors originating in non-gaseous contribution correction

The non-gaseous contribution correction is based on the linear interpolation of AECs obtained at the four window elements to cover the whole spectral range for the IR spectrometer. This systematically underestimates or overestimates gas concentrations in cases when the shape of the aerosol spectrum linearly interpolated is different from that of the real one.

An analysis of ILAS-II observational data only cannot give estimates of this type of errors. Therefore, simulations based on the same technique as in *Yokota et al.* [2002] have been carried out to give rough estimates of systematic errors caused by the non-gaseous contribution correction. In the present estimation, new complex refractive index data on absorption spectra of aerosols including PSCs from new laboratory experiments have been employed, i.e., the refractive index data from *Clapp et al.* [1995] for water ice, and from *Richwine et al.* [1995] for nitric acid trihydrate (NAT) were adopted, instead of the data from *Toon et al.* [1994].

Figure 7 shows the simulation results for the systematic errors, where the abscissa is magnitude of AEC at 780 nm and the ordinate is magnitude of the systematic errors

Fig. 7

estimated in terms of number density for the target gases. Different colors represent different aerosol and/or PSCs types, and different symbols do the assumed AEC profiles with different peak altitude. The effects of aerosols/PSCs on the errors of gas number density, due to the non-gaseous contribution correction, are almost linearly related to the extinction coefficient at 780 nm. Therefore, the results of linear regression for each aerosol/PSC type are also shown as regression lines in Figure 7. The slopes of the lines are given in Table 2 for convenience to carry out rough estimation of errors.

Table 2

The features of the systematic errors caused by the non-gaseous contribution errors are basically the same as those for ILAS [*Yokota et al.*, 2002], and some important points concerning O_3, HNO_3, N_2O, and CH_4 are as follows: First, the non-gaseous contribution correction has little effect on any gas profiles in the background sulfuric acid aerosol cases. On the other hand, a PSC layer of water ice with an extinction coefficient of 10^{-3} km^{-1} at 20 km causes a large artifact of a 0.74 ppmv overestimation of the retrieved O_3. For a NAT PSC layer with extinction coefficients of the order of 10^{-3} km^{-1}, gases HNO_3, N_2O, and CH_4 suffer from significant systematic errors (-0.96 ppbv for HNO_3, -43.0 ppbv for N_2O, and -0.48 ppmv for CH_4), which will not be negligible compared to the climatological values at 20 km. This means that the type of PSC has quantitative effects on the retrieved gas profiles.

6. Summary and Concluding Remarks

This paper describes the ILAS-II Version 1.4 data processing algorithm used to produce ILAS-II Version 1.4 data products, focusing mainly on its differences from the ILAS Version 5.20 algorithm. This paper also discusses the results of simulations for the systematic errors caused by the corrections to the IR spectrometer data to eliminate the non-gaseous contribution. The results provide rough estimates of the systematic errors which are inevitable when high density aerosols and/or PSCs are existing. ILAS-II data product users should be aware and careful about those systematic errors under some conditions.

This paper also gives results of measurement-error analyses for the ILAS-II Version 1.4 data products. The errors are expressed as total errors, which are comprised of the repeatability error and the external error. The repeatability error is estimated from the minimum extent of variability of measurements for a calm atmosphere, which can be regarded approximately as measurement precision due to the instrumental performance itself. On the other hand, the external errors are caused by the uncertainties of specified parameters brought in during the course of data processing, such as temperature uncertainty and non-gaseous contribution correction uncertainty.

The signals from the IR spectrometer and the SES were different from what had been

expected from the original design of the instrument. The detailed analyses of the processed data and the results of laboratory experiments using the ILAS-II Engineering Model revealed that the distortion of the reflective optics (mirror), in which rectangular holes are excavated as light entrance slits of the spectrometers, might have been their causes. Consequently, the problems in data processing have hindered successful data retrievals for some of the target gases. The Version 1.4 data products of O_3, HNO_3, N_2O, CH_4, and AEC at 780 nm are provided to the general public since the validation analyses have been completed for those parameters. Studies are underway for solving the problems above to lead to a revised and better version of the algorithm in the near future.

Acknowledgments. The authors would like to thank G. C. Toon for the pseudo-line parameters, S. A. Clough and ARM members for information on the H_2O continuum calculation (CKD2.4 of LBLRTM), L. S. Rothman and other HITRAN development members for information on the line parameter database, and R. Swinbank for the UKMO assimilation data of temperature and pressure. We are also grateful to Fujitsu F.I.P. Co. for their contribution to processing the ILAS-II data at the ILAS-II Data Handling Facility (ILAS-II DHF) of the National Institute for Environmental Studies (NIES). The ILAS-II project has been sponsored by the Ministry of the Environment (MOE), Japan. A part of

the research works was supported with the Global Environment Research Fund provided by the MOE. We gratefully thank to the ILAS-II Advisory Committee members, the ILAS-II Science Team members, and the ILAS-II Validation Experiment Team members for useful discussions and suggestions. Especially, we acknowledge NIES postdoctorial fellows, Y. Terao, H. Irie, M. Ejiri, N. Saitoh, and T. Tanaka for their efforts in discussions on algorithm improvements and data validations.

References

BIPM, IEC, IFCC, ISO, IUPAC, IUPAP and OIML (1993), *Guide to the Expression of Uncertainty in Measurement*, 100 pp., ISO/TAG4/WG3 Technical Advisory Group on Meteorology.

Camy-Peyret, C., S. Payan, P. Jeseck, Y. Té, and T. Hawat (2001), High resolution balloon-borne spectroscopy within the O_2 *A*-band: observations and radiative transfer modeling, IRS' 2000: Current Problems in Atmospheric Radiation, W. L. Smith and Yu. M. Timofeyev (Eds.). A. Deepak Publishing, Hampton, Virginia.

Clapp, M. L., Miller, R. E., and Worsnop, D. R. (1995), Frequency-dependent optical constants of water ice obtained directly from aerosol extinction spectra, *J. Phys. Chem.*, **99**, 6317-6326.

Clough, S. A., F. X. Kneizys, and R. W. Davis (1989), Line shape and the water vapor continuum, Atmos. Res., 23, 229–241.

Ejiri, M. K., et al., (2005), Validation of ILAS-II Version 1.4 nitrous oxide and methane profiles, this issue.

Hayashida, S., N. Saitoh, A. Kagawa, T. Yokota, M. Suzuki, H. Nakajima, and Y. Sasano (2000), Arctic polar stratospheric clouds observed with the Improved Limb Atmospheric Spectrometer during the winter of 1996/1997, *J. Geophys. Res.*, **105,** 24,715-24,730.

Irie, H., et al. (2005), Validation of stratospheric nitric acid concentration profiles observed by ILAS-II, this issue.

Irion, F. W., et al.(2002), Atmospheric Trace Molecule Spectroscopy (ATMOS) experiment

Version 3 data retrievals, *Appl. Opt.*, **41**, 6968-6979.

JAXA Earth Observation Center Ed. (2005), ADEOS-II Data Users Handbook, 2nd edition, (available from the web at; http://www.eoc.jaxa.jp/adeos2/adeos2_handbook_e.pdf).

Kurucz, T. L. (1992), Synthetic infrared spectra, *Infrared Solar Physics*, *IAU Symp. 154*, edited by D. M. Rabin and J. T. Jefferies, Kluwer, Acad., Norwell Massachusetts.

Lorenc, A. C., S. P. Ballard, R. S. Bell, N. B. Ingleby, P. L. F. Andrews, D. M. Barker, J. R. Bray, A. M. Clayton, T. Dalby, D. Li, T. J. Payne, and F. W. Saunders (2000), The Met. Office global three-dimensional variational data assimilation scheme, *Q. J. R. Meteorol. Soc.*, **126**(570), 2991-3012.

Nakajima, H., M. Suzuki, T. Yokota, T. Sugita, Y. Itou, M. Kaji, N. Araki, K. Waragai, H. Yamashita, H. Kanzawa, and Y. Sasano (2002), Tangent height registration for the solar occultation satellite sensor ILAS: A new technique for Version 5.20 products, *J. Geophys. Res*., **107**, 8215, doi:10.1029/2001JD000607.

Nakajima, H., et al. (2005), Characteristics and performance of the Improved Limb Atmospheric Spectrometer-II (ILAS-II) onboard the ADEOS-II satellite, this issue.

Rees, D., et al. (Ed.) (1990), COSPAR International Reference Atmosphere: 1986 Part II: Middle Atmosphere Model, *Adv*. *Space Res*., **10**, 520 pp.

Richwine, L. J., Clapp M. L., Miller, R. E., and Worsnop, D. R. (1995), Complex refractive indices in the infrared of nitric acid trihydrate aerosols, *Geophys. Res. Lett.*, **22**, 2625-2628.

Rothman, L. S., et al. (1998), The HITRAN molecular spectroscopic database and HAWKS (HITRAN atmospheric workstation): 1996 edition, *J. Quant. Spectrosc. Radiat. Transfer*, **60**, 665-710.

Rothman, L. S., et al. (2003), The HITRAN molecular spectroscopic database: edition of 2000 including updates through 2001, *J. Quant. Spectrosc. Radiat. Transfer*, **82**, 5-44.

Saitoh, N., et al. (2005), Intercomparison of ILAS-II Version 1.4 aerosol extinction coefficients at 780 nm with SAGE II, SAGE III, and POAM III aerosol data, this issue.

Sasano, Y. (2002), Preface, *J. Geophys. Res.*, 107(D24), 8204, doi:10.1029/2002JD002155.

Sugita, T., T. Yokota, H. Nakajima, H. Kobayashi, N. Saitoh, H. Kawasaki, M. Usami, H. Saeki, M. Horikawa, and Y. Sasano (2004), A comparative study of stratospheric temperatures between ILAS-II and other data, *Proc. of SPIE*, **5652**, 279-289.

Sugita, T., et al. (2005), Ozone profiles in the high-latitude stratosphere and the lower mesosphere measured by the Improved Limb Atmospheric Spectrometer (ILAS)-II: Comparison with other satellite sensors and ozonesondes, this issue.

Swinbank, R., and A. O'Neill (1994), A stratosphere-troposphere data assimilation system, *Mon. Weather Rev.*, 122, 686-702.

Tanaka, T., H. Nakajima, T. Sugita, M. K. Ejiri, H. Irie, N. Saitoh, Y. Terao, H. Kawasaki, M. Usami, T. Yokota, H. Kobayashi, and Y. Sasano (2005), New tangent height registration method with Version 1.4 data retrieval algorithm for the solar occultation sensor ILAS-II, this issue.

Toon, O. B., et al. (1994), Infrared optical constants of H2O ice, amorphous nitric acid solutions, and nitric acid hydrates, *J. Geophys. Res.*, **99**, 25,631-25,654.

Wagner, G. and M. Birk (2003), New infrared spectroscopic database for chlorine nitrate, *J. Quant. Spectrosc. Radiat. Transfer*, **82**, 443-460.

Yokota, T., H. Nakajima, T. Sugita, H. Tsubaki, Y. Itou, M. Kaji, M. Suzuki, H. Kanzawa, J. H. Park, Y. Sasano (2002), Improved Limb Atmospheric Spectrometer (ILAS) data retrieval algorithm for Version 5.20 gas profile products, *J. Geophys. Res.*, **107(D24)**, 8216, 10.1029/2001JD000628.

Tables

Table 1 ILAS-II instrument characteristics

Parameter	Infrared (IR) spectrometer	Mid-infrared (MIR) spectrometer	High resolution infrared (HRIR) spectrometer	Visible (VIS) spectrometer	Sun-Edge Sensor (SES)
Spectral range	6.21-11.76 μm	3.00-5.70 μm	12.78-12.85 μm	753-784 nm	1050 nm
	850-1610 cm^{-1}	1754-3333 cm^{-1}	778-782 cm^{-1}	12755-13280 cm^{-1}	-
No. of elements	44	22	22	1024	1024
Resolution	0.129 μm	0.129 μm	0.0032 μm	0.15 nm	8.185 arcsec
Entrance slit (V×H) at a tangent point	1.0 × 13.0 km	1.0 × 13.0 km	1.0 × 21.7 km	1.0 × 2.0 km	1.0 × 13.0 km
Sampling frequency	10 Hz				
Data rate	453.7 Kbps				
Chopper frequency	30 Hz for IR, MIR, and HRIR spectrometers				
Size (W×D×H)	950 × 1670 × 600 mm				
Weight	138 kg				
Power	120 W (maximum)				

Table 2 Estimates of systematic errors remaining after the non-gaseous correction at an altitude of 20 km for ILAS-II standard gas products

	O_3				HNO_3			
	a	±1 σ S.D.	cm^{-3}	ppmv	*a*	±1 σ S.D.	cm^{-3}	ppbv
S(75)	-4.98E+13	6.43E+11	-2.49E+10	-0.015	3.10E+11	3.67E+09	1.55E+08	0.093
S(50)	2.02E+14	1.82E+12	1.01E+11	0.060	8.97E+10	2.79E+09	4.49E+07	0.027
ICE	1.24E+15	4.05E+13	1.24E+12	0.744	2.36E+11	2.60E+10	2.36E+08	0.141
NAT	1.48E+14	1.21E+13	1.48E+11	0.088	-1.60E+12	4.00E+10	-1.60E+09	-0.957
STS(a)	5.16E+12	1.17E+12	5.16E+09	0.003	-8.79E+09	1.07E+10	-8.79E+06	-0.005
STS(b)	2.31E+14	1.21E+13	2.31E+11	0.138	1.24E+11	2.12E+09	1.24E+08	0.074
STS(c)	2.49E+14	1.27E+13	2.49E+11	0.149	1.98E+11	4.11E+09	1.98E+08	0.118
STS(d)	2.18E+14	1.02E+13	2.18E+11	0.130	1.99E+11	6.91E+09	1.99E+08	0.119

	N_2O				CH_4			
	a	±1 σ S.D.	cm^{-3}	ppbv	*a*	±1 σ S.D.	cm^{-3}	ppmv
S(75)	2.68E+13	1.55E+12	1.34E+10	8.04	-2.89E+14	3.85E+12	-1.45E+11	-0.087
S(50)	1.09E+13	1.00E+12	5.45E+09	3.26	-1.97E+14	2.27E+12	-9.83E+10	-0.059
ICE	3.06E+12	1.91E+11	3.06E+09	1.84	-5.51E+13	4.56E+12	-5.51E+10	-0.033
NAT	-7.19E+13	6.82E+12	-7.19E+10	-43.0	8.04E+14	5.18E+13	8.04E+11	0.482
STS(a)	-1.54E+13	1.21E+12	-1.54E+10	-9.22	2.60E+14	1.18E+13	2.60E+11	0.156
STS(b)	8.33E+12	2.11E+12	8.33E+09	4.99	-1.15E+14	7.31E+12	-1.15E+11	-0.069
STS(c)	1.52E+13	3.37E+12	1.52E+10	9.08	-1.96E+14	1.14E+13	-1.96E+11	-0.117
STS(d)	1.14E+13	3.52E+12	1.14E+10	6.85	-1.22E+14	6.36E+12	-1.22E+11	-0.073

The regression coefficient *a* is a proportional factor that relates the systematic error of the number density of a gas to the 780 nm aerosol extinction coefficient, as shown in Figure 7. Typical values for systematic errors in concentrations (cm^{-3}) and volume mixing ratios (ppmv) at a tangent altitude of 20 km are also listed for cases of the extinction coefficient value at 780 nm of 5.0×10^{-4} km^{-1} for sulfuric acid aerosols and of 1.0×10^{-3} km^{-1} for PSCs. The component ratios are as follows: STS(a): 5 wt%H_2SO_4/37 wt%HNO_3/H_2O, STS(b):33 wt%H_2SO_4/15 wt% HNO_3/H_2O, STS(c):47 wt%H_2SO_4/3 wt%HNO_3/H_2O, and STS(d):60 wt%H_2SO_4/0.5 wt%HNO_3/H_2O. S(50) and S(75) are sulfuric acid aerosols whose components are 50 wt%H_2SO_4/H_2O and 75 wt%H_2SO_4/H_2O, respectively.

Figure Captions

Figure 1

Data sequence of ILAS-II measurements: [top left chart: sunrise mode of the IR data, top right chart: sunset mode of the IR data, bottom left chart: sunrise mode of the VIS data, and bottom right chart: sunset mode of the VIS data]. (**a**: 0 % level signal part before measurement, **b**: atmospheric measurement part, **c**: 100 % level signal part, **d**: sun scan part, **e**: 0 % level signal part after measurement)

Figure 2

A schematic of time sequence of the AC mode signal sampling of the ILAS-II Level 0 data. An equivalent signal to the DC mode signal is created from the AC signals (shown by black dots in this figure) at four different phase angles.

Figure 3

An example of effective vertical resolutions (full width at half maximum: FWHM) of the instantaneous field of view (IFOV) versus tangent altitude for the ILAS-II sunrise mode. The solid curve shows the FWHM of the effective vertical resolutions of the IFOV as a

function of altitudes. The dotted curve denotes a 4-th polynomial curve fitted to the data. Similar results are obtained for the sunset mode.

Figure 4

An example of the search for the repeatability index for each altitude for ozone in the northern hemisphere. The minimum value of the relative standard deviation (S.D./mean) during April to October 2003 is selected as the repeatability index for each altitude, e.g., " † " represents the selected repeatability index as the minimum value at an altitude of 15 km.

Figure 5

Profiles of the repeatability error and the total error using a relative error (%) scale for the four gases and the AEC at 780 nm for the northern hemisphere (i.e., sunrise mode).

Figure 6

As in Figure 5, but for the southern hemisphere (i.e., sunset mode).

Figure 7

Systematic errors caused by the non-gaseous contribution correction for the ILAS-II gas products as a function of the extinction coefficient at 780 nm for various aerosols and PSCs at altitudes of 15, 20, and 25 km. The calculated systematic errors in gas number density (cm^{-1}) are presented as symbols with linear regression lines. The scales of volume mixing ratios (ppmv) for altitudes of 15, 20, and 25 km are also shown at the right-hand side of each chart. The component ratios from STS(a) to STS(d) are described in Table 2.

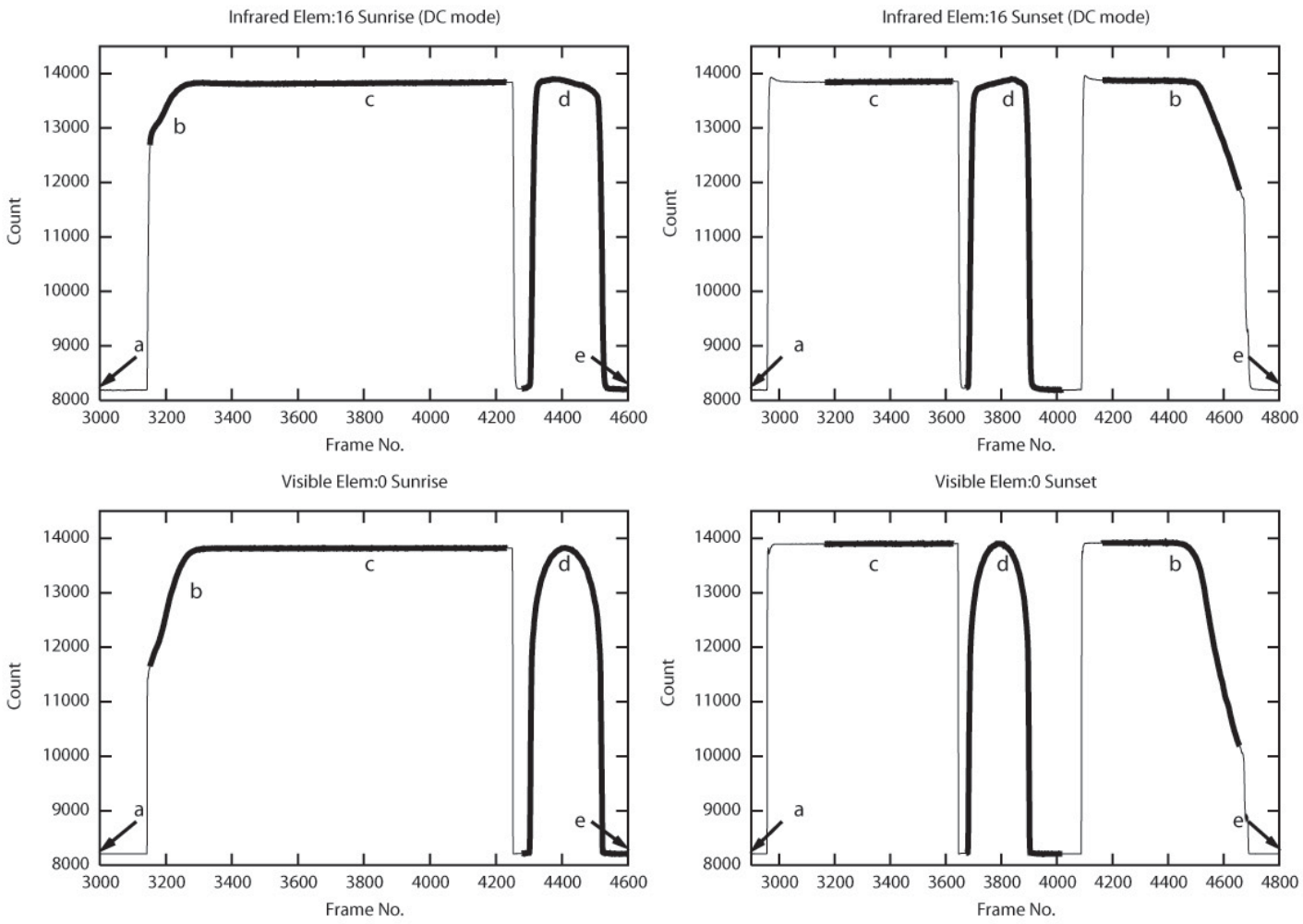
Infrared Elem:16 Sunrise (DC mode)
Infrared Elem:16 Sunset (DC mode)
Visible Elem:0 Sunrise
Visible Elem:0 Sunset
Count
Frame No.
a
b
c
d
e

Figure 1

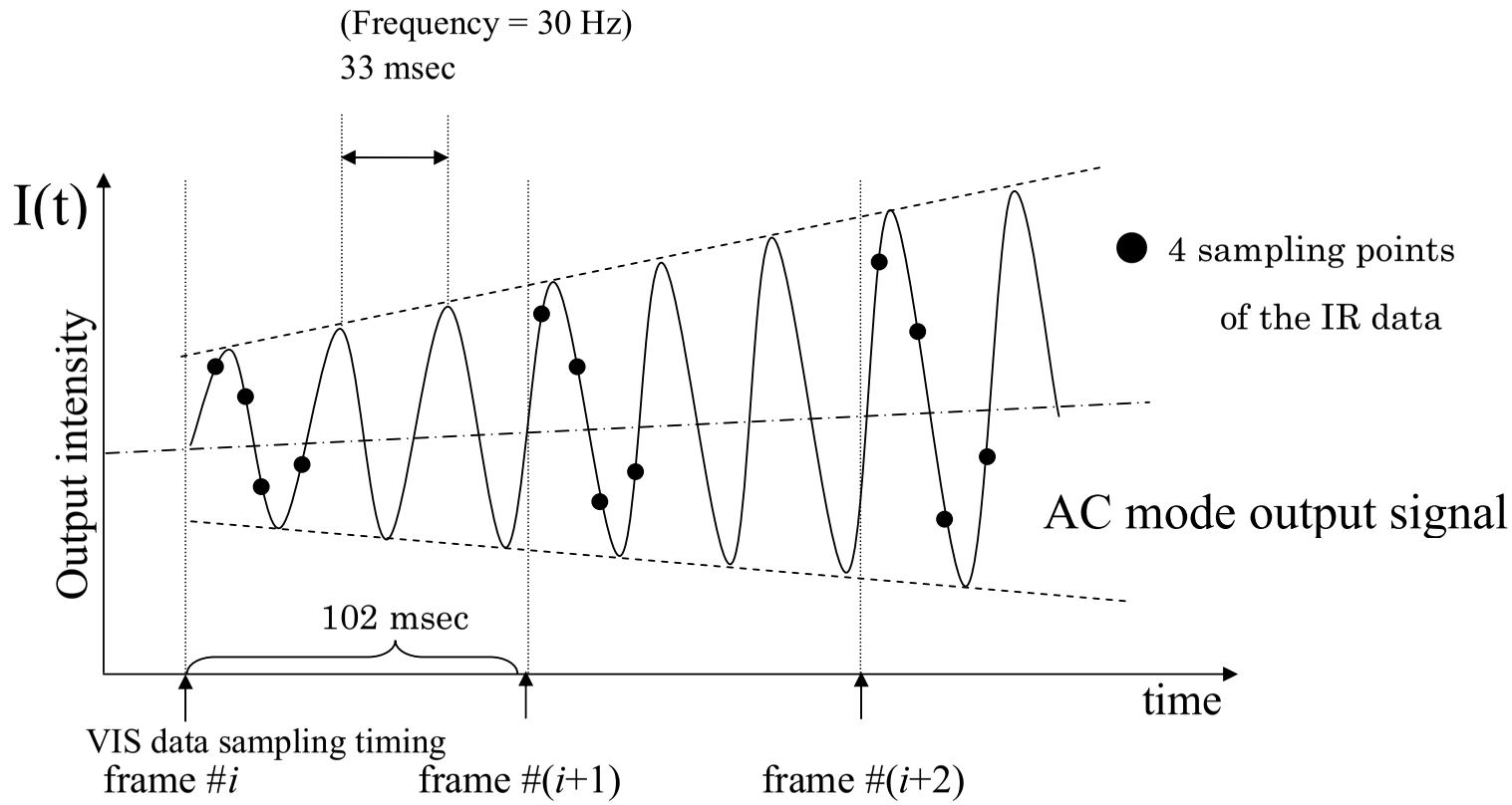
(Frequency = 30 Hz)
33 msec
I(t)
Output intensity
4 sampling points
of the IR data
AC mode output signal
102 msec
time
VIS data sampling timing
frame #i
frame #(i+1)
frame #(i+2)

Figure 2

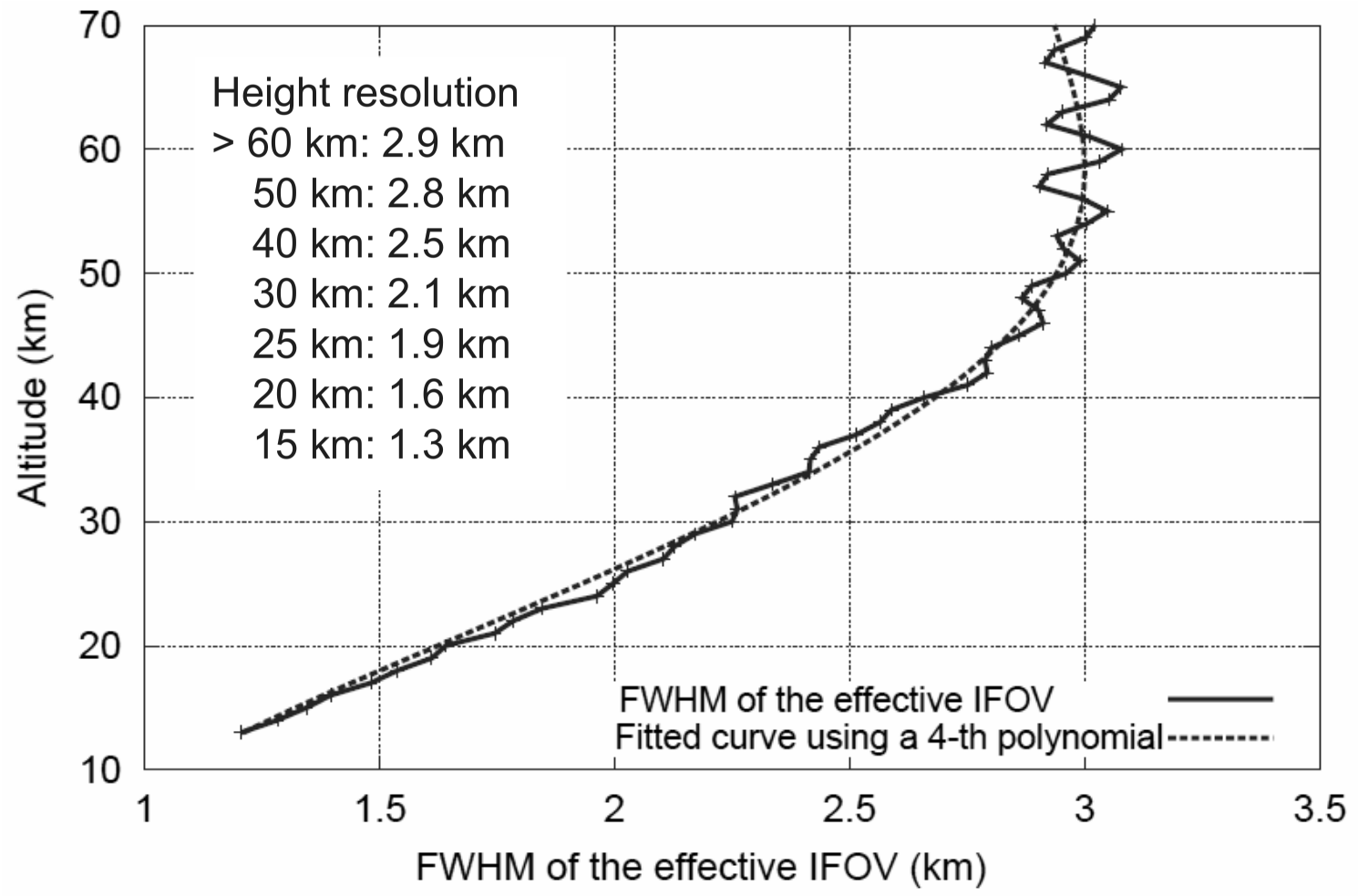
Height resolution
> 60 km: 2.9 km
50 km: 2.8 km
40 km: 2.5 km
30 km: 2.1 km
25 km: 1.9 km
20 km: 1.6 km
15 km: 1.3 km
FWHM of the effective IFOV
Fitted curve using a 4-th polynomial
Altitude (km)
FWHM of the effective IFOV (km)
70
60
50
40
30
20
10
1
1.5
2
2.5
3
3.5

Figure 3

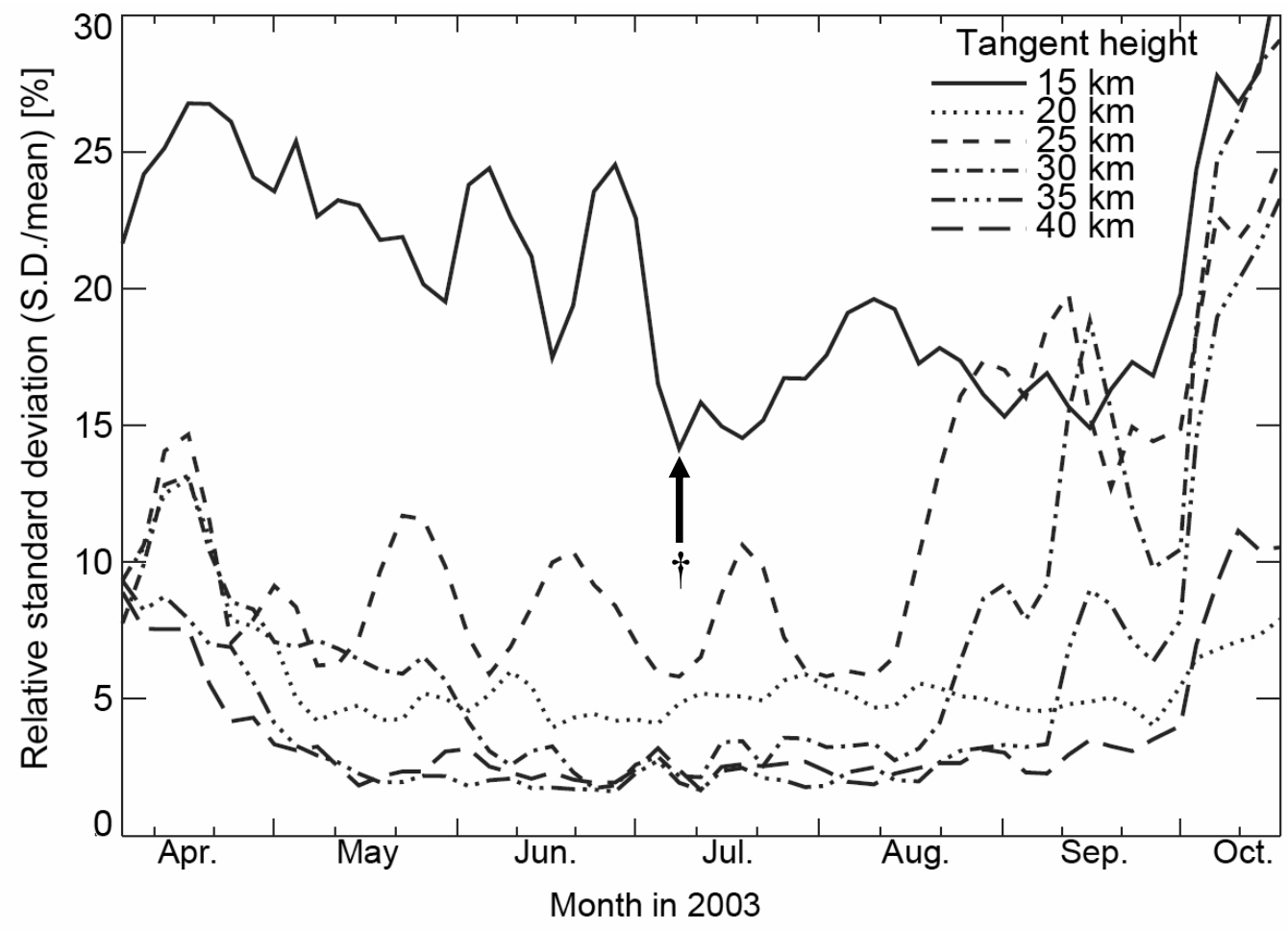
Tangent height
15 km
20 km
25 km
30 km
35 km
40 km
Relative standard deviation (S.D./mean) [%]
0
5
10
15
20
25
30
Apr.
May
Jun.
Jul.
Aug.
Sep.
Oct.
Month in 2003

Figure 4

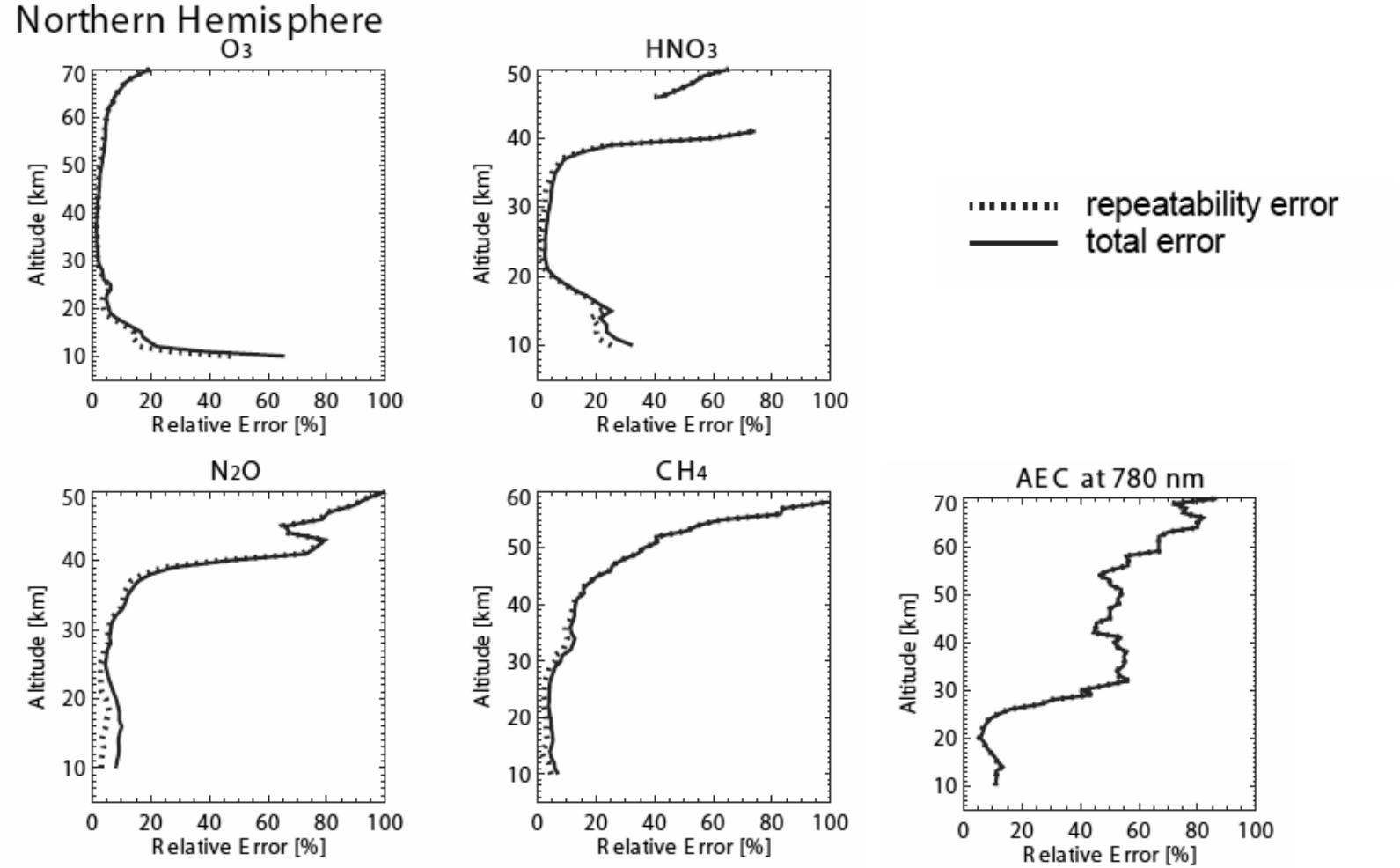
Northern Hemisphere
O3
HNO3
N2O
CH4
AEC at 780 nm
Altitude [km]
Relative Error [%]
repeatability error
total error

Figure 5

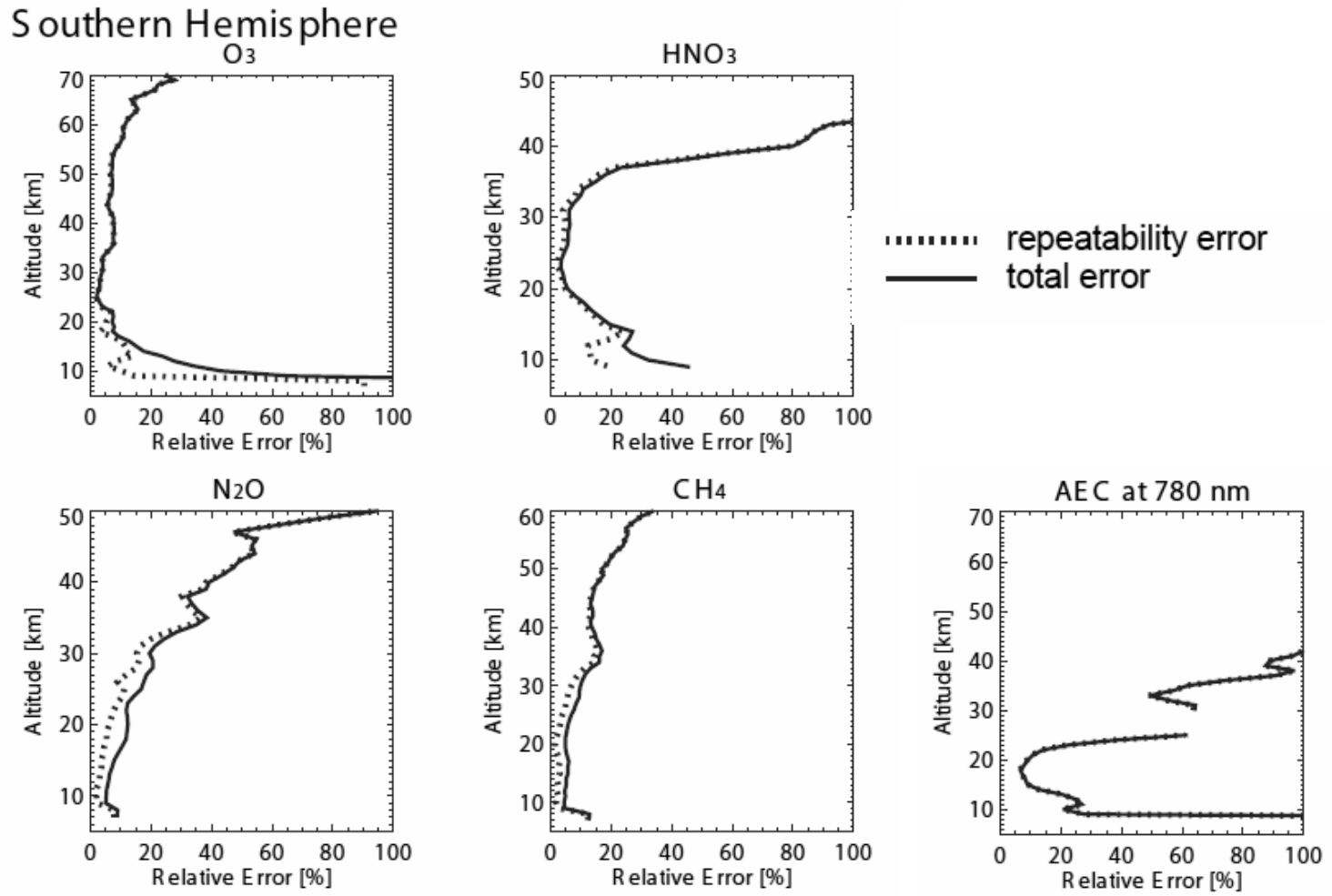
Southern Hemisphere
O3
HNO3
N2O
CH4
AEC at 780 nm
Altitude [km]
Relative Error [%]
repeatability error
total error

Figure 6

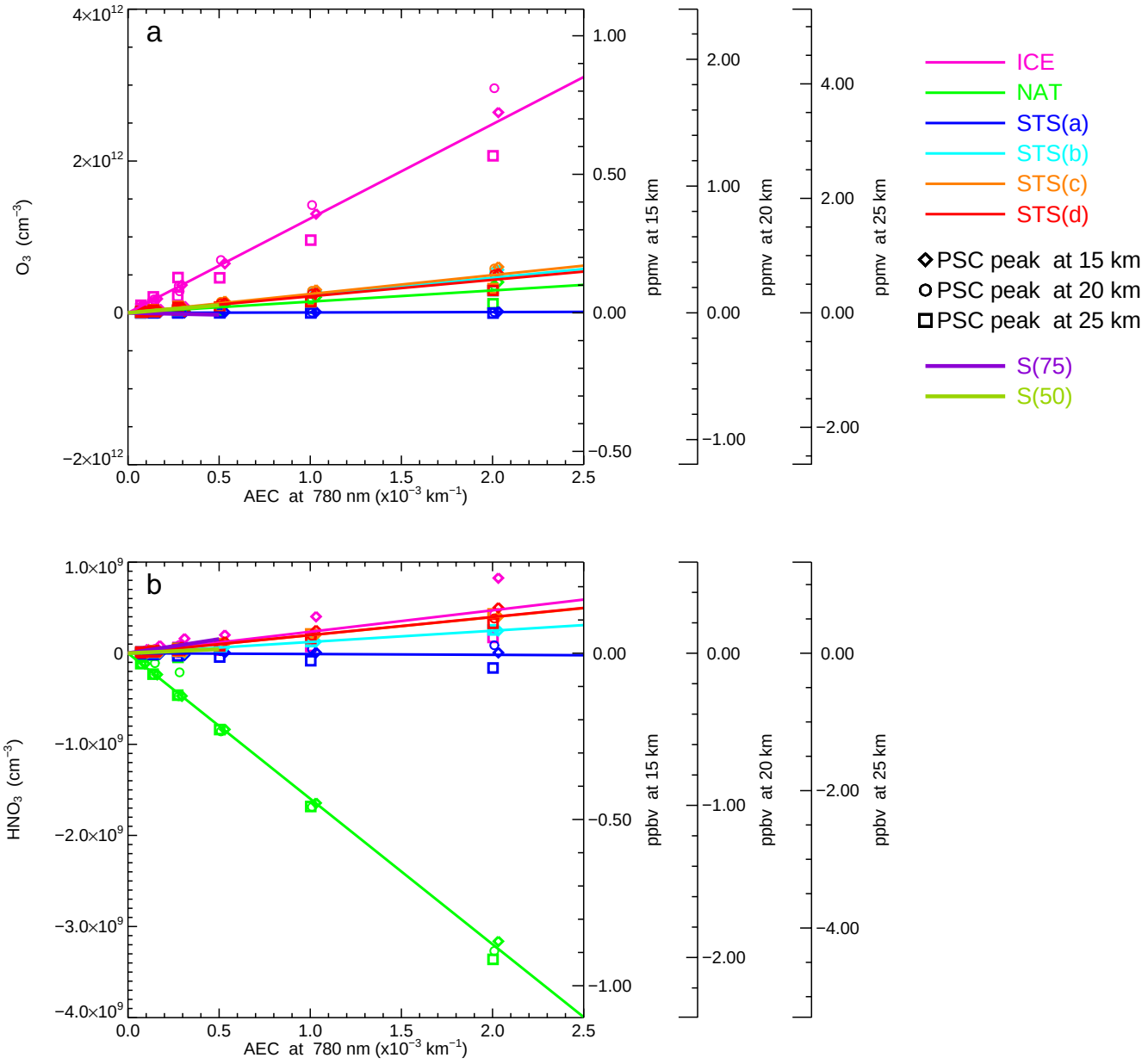
a
b
ICE
NAT
STS(a)
STS(b)
STS(c)
STS(d)
PSC peak at 15 km
PSC peak at 20 km
PSC peak at 25 km
S(75)
S(50)
O3 (cm-3)
HNO3 (cm-3)
ppmv at 15 km
ppmv at 20 km
ppmv at 25 km
ppbv at 15 km
ppbv at 20 km
ppbv at 25 km
AEC at 780 nm (x10-3 km-1)

Figure 7

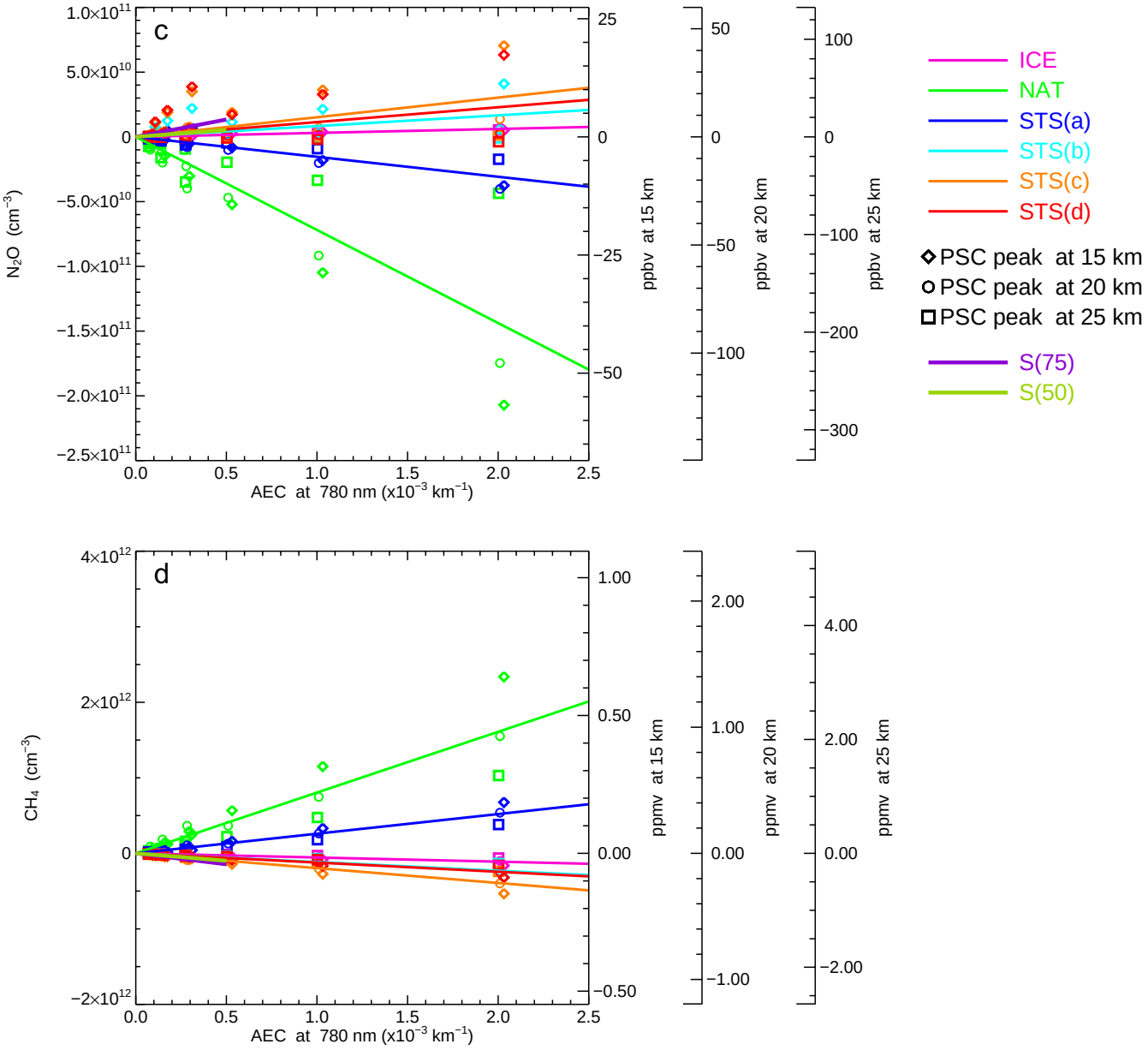

Figure 7 (cont.)